World Electric Vehicle Journal

MDPI

Article

Energy Management Strategy for P1 + P3 Plug-In Hybrid Electric Vehicles

Bo Zhang, Peilin Shi *, Xiangli Mou, Hao Li, Yushuai Zhao and Liaodong Zheng

School of Transportation and Vehicle Engineering, Shandong University of Technology, Zibo 255030, China; zhangbo121416@outlook.com (B.Z.); 15169284600@163.com (X.M.); 17659936128@163.com (H.L.); 13905489715@163.com (Y.Z.); 15083008238@163.com (L.Z.)

* Correspondence: shipl@sdut.edu.cn

Abstract: In order to simultaneously improve the fuel economy and overall performance of plug-in hybrid electric vehicles (PHEVs), this study selected the P1 + P3 configuration as its research object. Through a configuration analysis of hybrid vehicles, it confirmed the feasibility of P1 + P3 configuration-PHEV operating modes. Based on this, a rule-based control strategy was developed, and simulation models for the entire vehicle and control strategy were constructed in both Cruise and MATLAB/Simulink software. The study conducted simulation analysis by combining three sets of Worldwide Harmonized Light vehicles Test Cycle (WLTC) driving cycles to assess the fuel-saving potential of the dual-motor P1 + P3 configuration. The simulation results showed that the vehicle model was reasonably constructed and the proposed control strategy had good control effects on the entire vehicle. Compared to conventional gasoline vehicles, the P1 + P3 configuration PHEV achieved a 67.4% fuel economy improvement, demonstrating a significant enhancement in fuel efficiency with the introduction of electric motors.

Keywords: plug-in hybrid electric vehicle; energy management; rule-based control; logical thresholds; fuel economy

Citation: Zhang, B.; Shi, P.; Mou, X.; Li, H.; Zhao, Y.; Zheng, L. Energy Management Strategy for P1 + P3 Plug-In Hybrid Electric Vehicles. *World Electr. Veh. J.* **2023**, *14*, 332. https://doi.org/10.3390/wevj14120332

Academic Editor: Joeri Van Mierlo

Received: 2 November 2023
Revised: 24 November 2023
Accepted: 28 November 2023
Published: 30 November 2023

1. Introduction

The transportation sector is considered a major contributor to exacerbating climate change, for instance, through increased levels of carbon dioxide and the depletion of finite petroleum supplies. Extensive research has been conducted to seek alternatives to conventional automobiles, and the plug-in hybrid electric vehicle (PHEV) has emerged as a viable solution [1–5]. PHEVs typically combine a conventional internal combustion engine (ICE) propulsion system with a battery-powered electric propulsion system. These vehicles inherit the advantages of both traditional ICE vehicles and battery electric vehicles. In comparison to purely electric cars, PHEVs notably excel in their impressive range and the flexibility of their component sizing. Over the past decade, there has been a notable increase in the commercial success and market penetration of plug-in hybrid electric vehicles.

Despite achieving this success, there remains a continued need to enhance the plug-in hybrid electric vehicle (PHEV) for higher levels of fuel economy to bolster its competitiveness, presenting an ongoing challenge. Among various potential areas for improvement, energy management systems offer promising prospects for further advancements in cost-effectiveness [6,7]. Merely through algorithmic alterations in the operation and interaction of existing components within the powertrain, these systems can elevate the overall efficiency of PHEVs.

In the past, diverse energy management systems for hybrid vehicles have been developed, encompassing both optimization-based and rule-based control strategies [8–20]. Optimization-based energy management systems derive power distribution rules among multiple energy sources by solving intricate optimization problems, whereas rule-based systems primarily rely on heuristics.

Global optimization methods such as dynamic programming (DP) and Pontryagin's minimum principle (PMP) aim to maximize fuel economy by minimizing cost functions representing fuel consumption and emissions along a given driving cycle [13–15]. However, these techniques cannot be directly applied to real vehicles due to their inability to precisely anticipate the entire driving cycle in advance. Therefore, global optimization methods are commonly utilized as benchmarks to evaluate other energy management systems. To address these challenges, the finite-horizon model predictive control (MPC) method is employed to balance real-time implementation with controller optimization [16–19]. However, it necessitates predicting or identifying future driving cycles in advance.

Rule-based energy management strategies can be further classified through deterministic and fuzzy logic. Deterministic rules are crafted to enhance fuel efficiency while minimizing transmission losses and emissions by mapping the efficiency regions of Internal Combustion Engines (ICEs) and electric motors (EMs). They rely on empirical knowledge and optimal operational points. They can be primarily categorized into the following types:

The Thermostat (ON/OFF) strategy utilizes the generator and ICE to produce electrical energy. This method maintains battery SoC between predefined upper and lower limits at all times. However, it suffers from the drawback of not being able to supply the needed power to the vehicle in all modes [21–24].

The Power Follower strategy, also known as the baseline strategy, relies on the generator and Internal Combustion Engine (ICE) as the main power sources. It operates by responding to the driver's power requirements. The rules governing this strategy are formulated using heuristics and human intelligence. In this technique, the EM only works as an auxiliary power source. The ICE and the generator work as the primary sources, and the EM only aids the ICE. This is used in series and parallels HEVs [25].

The State Machine (Multimode) strategy operates within specific vehicle states using an algorithm based on a decision tree of stable conditions. It encompasses various modes of operation: ICE only mode, where only the Internal Combustion Engine (ICE) propels the vehicle; boost mode, utilizing both the ICE and the Electric Motor (EM) for driving force; and charging mode, where the ICE charges the vehicle while simultaneously propelling it. This strategy, also known as the Multimode strategy, adapts to distinct vehicle conditions by employing different operational modes to optimize overall performance [26,27].

The fuzzy logic strategy relies on if–then rules. Its effectiveness hinges on the selection of membership functions and the precise formation of fuzzy rules [28]. Rule formation involves engineers' reasoning. Fuzzy logic primarily comprises optimized fuzzy rule control, adaptive fuzzy logic control, and predictive fuzzy logic control. The first type employs optimization algorithms to adjust membership functions within fuzzy logic, such as divided rectangle (DIRECT), particle swarm optimization (PSO), and the genetic algorithm (GA) [29]. The second type possesses adaptive capabilities but requires prior knowledge or data to act upon [30–32]. The third type can predict the state of power transmission systems and take real-time action, but necessitates the use of a Global Positioning System (GPS) for vehicle tracking, relying on known trip-related information [33].

Building upon the aforementioned discussion, the development of a rule-based energy management strategy tailored for the complex P1 + P3 hybrid architecture in automobiles holds significant research value due to its low computational load, independence from predictive loops, and closer alignment with practical applications. This study designs the operational modes of the P1 + P3 plug-in hybrid electric vehicle (PHEV) based on the engine characteristic curves. Building upon this, this research develops an energy management strategy using the State Machine (Multimode) strategy to ensure the vehicle maintains higher overall efficiency across various operating modes. To achieve this, we constructed the entire vehicle model using Cruise software and developed an energy management strategy model using MATLAB/Simulink software. We conducted simulations to analyze the rationality of the designed control strategy under different operating conditions and assessed the impact of the dual motors in the P1 + P3 configuration on the vehicle's energy and economic performance.

2. Materials and Methods

2.1. Structure of the P1 + P3 Plug-in Hybrid Powertrain System

As shown in Figure 1, a simplified diagram of the P1 + P3 dual-motor hybrid powertrain structure is presented. The system includes components such as an engine, a P1 motor, a P3 motor, a clutch, transmission, and a main reducer.

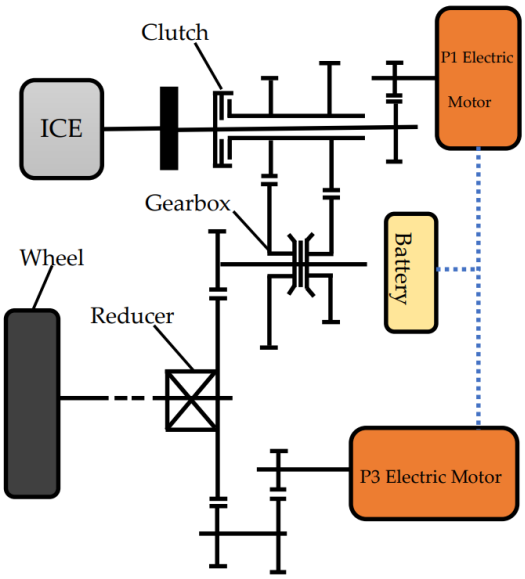

Figure 1. Structure of the P1 + P3 PHEV configuration.

The P1 + P3-configuration PHEV system's power can be provided by the engine, the P1 motor, and the P3 motor. The P1 motor is installed at the rear of the engine and carries out functions like engine idle start–stop, engine speed control, and driving the electrical components of the vehicle independently. The P3 motor is located between the differential and the transmission and is directly connected to the transmission output shaft through a reduction mechanism. It also features regenerative braking capabilities. When the clutch is disengaged and the transmission is in neutral, the vehicle is driven solely by the P3 motor via a two-stage gear mechanism. When the clutch is engaged and the transmission is in gear, the P3 motor can work in conjunction with the engine to drive the vehicle, or the vehicle can be solely driven by the engine while the P3 motor idles without torque output. The engine can also drive the P1 motor to power the vehicle and charge the power battery, enabling a driving and charging mode. During deceleration and downhill driving, the clutch disengages, allowing for efficient energy recovery by the P3 motor. Furthermore, the three power sources can be coordinated and controlled according to the vehicle's torque demands and its state under different operating conditions.

Based on the preceding discussion, this study categorizes the driving modes of the P1 + P3 plug-in hybrid electric vehicle into six types:

EM alone: sole propulsion provided by the P3 motor.

Extended-range mode: sole propulsion by the P3 motor with the engine generating power via fuel to charge the battery (P1 motor becomes generator).

ICE alone: sole propulsion by the engine.

Combined ICE-EM: propulsion provided jointly by the engine and motor.

Power split: division of the engine power between driving the vehicle and charging the battery.

Regenerative braking: during vehicle deceleration, the P3 motor recovers braking energy to recharge the battery.

Table 1 provides the operational status of key components under different driving modes.

Table 1. Working status of various components in different modes.

Operating Modes	Status of Key Components				
	Engine	P1 Motor	P3 Motor	Power Battery	Clutch
EM alone	OFF	OFF	ON	discharged	disengaged
Extended-range mode	ON	ON	ON	charged	engaged
ICE alone	ON	OFF	OFF	idle	engaged
Combined ICE-EM	ON	ON	OFF	discharged	engaged
Power split	ON	ON	OFF	charged	engaged
Regenerative braking	OFF	OFF	ON	charged	disengaged

2.2. Rule-Based Energy Management Strategy

An energy management strategy, as one of the key technical aspects of PHEVs, can be formulated based on variations in vehicle power requirements and the battery's state of charge (SOC) to optimize its operation.

2.2.1. Low- to Mid-Speed Phase

When driving in suburban conditions, vehicle speeds are relatively low, and power demands are minimal. To improve fuel economy, it is advantageous to use the electric motor as the primary power source whenever possible. The subject of this study is the P1 + P3 hybrid powertrain configuration. During the low- to mid-speed phases, the operating modes include EM alone, extended-range mode, and regenerative braking mode.

In suburban driving conditions, if the battery is adequately charged, and the electric motor can provide the required torque for the driver, the EM alone is given priority. If the battery's state of charge (SOC) falls below SOC min, then the extended-range mode is engaged. During braking situations, following the principle of maximizing regenerative braking, if the required braking torque is minimal, priority is given to the P3 motor for regenerative braking. When there is significant deceleration and the P3 motor can provide the maximum braking torque while ensuring safety, mechanical braking is used to complement the remaining braking force requirements, thus maximizing energy recovery [34]. If the battery's charge is sufficient, the mechanical brake is employed to ensure that the battery is not overcharged. The logic for switching vehicle operating modes during the low-speed phase and torque allocation are depicted in Table 2.

Table 2. Mode switching logic and torque allocation during low- to mid-speed phases.

Operating Modes	Switching Logic		Torque Allocation
	Condition 1	Condition 2	
EM alone	$SOC > SOC_{min}$	$T_{req} \leq T_{P3\_max}$	$T_{eng} = 0$
			$T_{P1} = 0$
			$T_{P3} = T_{req}$
Extended-range mode	$SOC \leq SOC_{min}$	—	$T_{eng} = T_{eng\_opt}$
			$T_{P1} = T_{eng\_opt}$
			$T_{P3} = T_{req}$
Regenerative braking	$SOC \leq SOC_{max}$	$T_{req} \leq T_{P3\_max}$	$T_{eng} = 0$
			$T_{P1} = 0$
			$T_{P3} = T_{req}$
		$T_{req} > T_{P3gen\_max}$	$T_{eng} = 0$
			$T_{P1} = 0$
			$T_{P3} = T_{P3gen\_max}$

The switching control logic for low-speed phase operating modes is illustrated in Figure 2. This switching logic can be divided into three layers:

1. Determining whether the vehicle operates in driving mode or regenerative braking mode based on the overall vehicle torque demand.
2. Deciding whether to enter EM alone or extended-range mode and whether to engage energy recovery based on SOC status.
3. Based on the maximum regenerative braking capability of the P3 motor, determining whether to engage in blended braking.

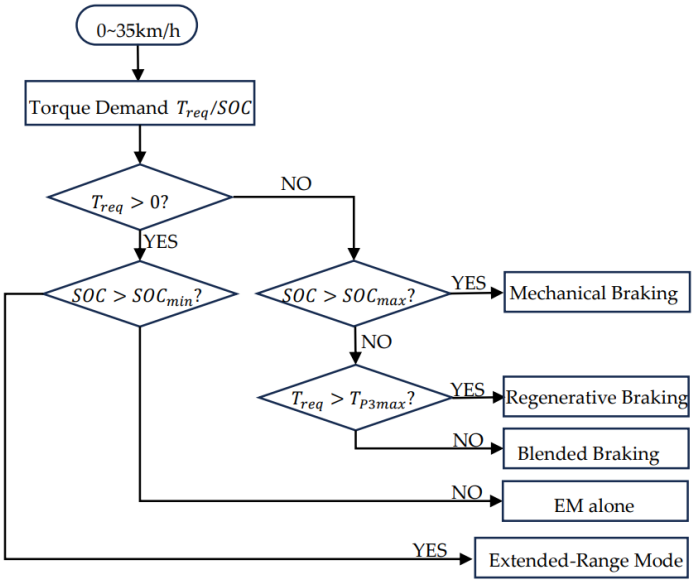

Figure 2. Control strategy flow for low- to mid-speed phases.

2.2.2. High-Speed Phase

When the vehicle is operating at high speeds and requires significant power, it enters the high-speed mode. In this mode, the engine serves as the primary power source to propel the vehicle, and both the P1 motor and P3 motor can function as drive motors or generators. Figure 3 illustrates the operational range and efficiency of the engine. The green area represents the high-efficiency region, while the red area signifies the low-efficiency region. The 'opt' curve indicates the engine's optimal operating curve, obtained through laboratory testing.

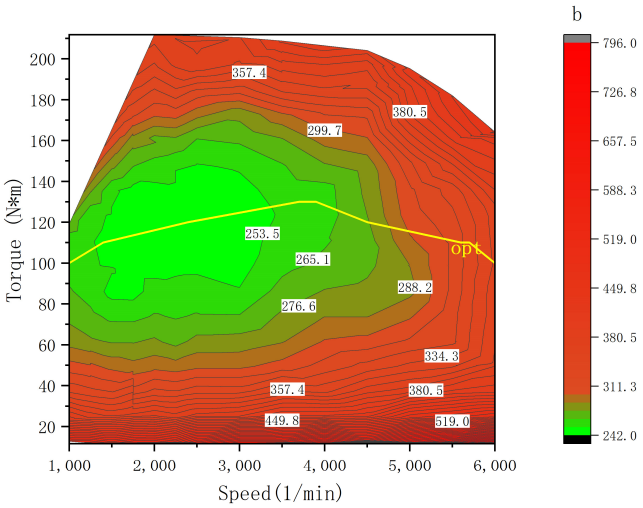

Figure 3. Engine characteristics chart.

Because the high-speed phase primarily relies on the engine for propulsion, there are four main operating modes during this phase: ICE alone, combined ICE-EM, power split, and regenerative braking, with the latter being the same as in the low- to mid-speed phase. The conditions and torque allocation for different operating modes during this phase are detailed in Table 3.

Table 3. Mode switching logic and torque allocation during high-speed phase.

Operating Modes	Switching Logic		Torque Allocation
	Condition 1	Condition 2	
ICE alone	$0 < SOC \leq SOC_{min}$	$T_{req} > T_{eng\_opt}$	$T_{eng} = min(T_{req}, T_{engmax})$
			$T_{P1} = 0$
			$T_{P3} = 0$
Combined ICE-EM	$SOC > SOC_{min}$	$T_{eng\_opt} < T_{req} \leq T_{eng\_max}$	$T_{eng} = T_{eng\_opt}$
			$T_{P1} = T_{req}$-T_{eng_opt}
			$T_{P3} = 0$
		$T_{req} > T_{eng\_max}$ $T_{req} \leq T_{cb1}$	$T_{eng} = T_{req} - T_{P1\_max}$
			$T_{P1} = T_{cb2}$
			$T_{P3} = 0$
		$T_{req} > T_{eng\_max}$ $T_{req} > T_{cb1}$	$T_{eng} = T_{req} - T_{P1\_max}$
			$T_{P1} = T_{P1\_max}$
			$T_{P3} = 0$
Power split	$0 < SOC \leq SOC_{max}$	$T_{eng\_min} < T_{req} \leq T_{eng\_opt}$ $T_{cb2} \leq T_{P1gen\_max}$	$T_{eng} = T_{eng\_opt}$
			$T_{P1} = T_{cb2}$
			$T_{P3} = 0$
		$T_{eng\_min} < T_{req} \leq T_{eng\_opt}$ $T_{cb2} > T_{P1gen\_max}$	$T_{eng} = T_{eng\_opt} - T_{P1gen\_max}$
			$T_{P1} = T_{P1gen\_max}$
			$T_{P3} = 0$
Regenerative braking		$T_{req} < 0$	$T_{eng} = 0$
			$T_{P1} = 0$
			$T_{P3} = max(T_{req}, T_{P3gen\_max})$

In the table, T_{cb1} represents the sum of the engine's optimal torque and the maximum drive torque of the P3 motor, as expressed in Formula (1):

$$T_{cb1} = T_{eng\_opt} + T_{P3\_max} \quad (1)$$

T_{cb2} represents the difference between the engine's optimal drive torque at the current speed and the vehicle's torque demand, as described in Formula (2):

$$T_{cb2} = T_{eng\_opt} - T_{req} \quad (2)$$

Based on the above analysis, the control strategy workflow for the high-speed phase can be depicted as shown in Figure 4.

In the control strategy, the torque values of all power sources are converted to the torque transmitted to the wheel ends. The threshold parameters in the control strategy are as presented in Table 4.

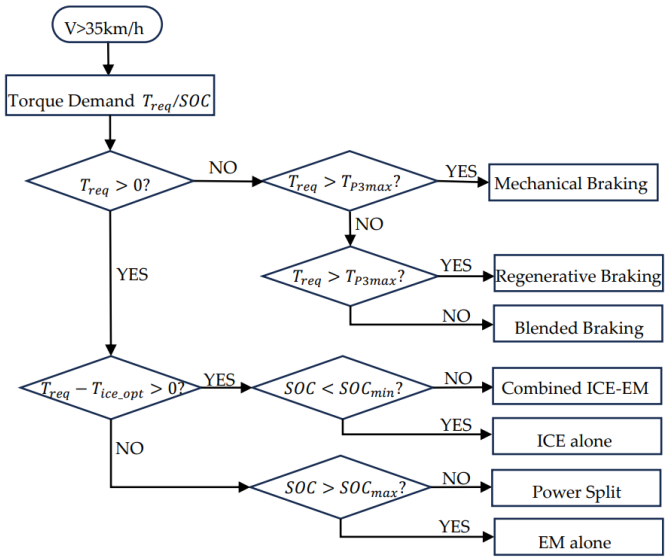

Figure 4. Control strategy workflow for high-speed phase in PHEV.

Table 4. Physical meanings of parameters in the control strategy.

Variable Names	Variable Descriptions
SOC_{min}	Minimum SOC threshold value
SOC_{max}	Maximum SOC threshold value
T_{req}	Vehicle wheel-end torque demand
T_{eng_max}	Engine maximum torque
T_{eng_min}	Engine minimum operating torque threshold value
T_{eng_opt}	Engine high-efficiency zone optimal torque
T_{P1gen_max}	P1 motor maximum regenerative torque
T_{P1_max}	P1 motor maximum drive torque
T_{P3gen_max}	P3 motor maximum regenerative torque
T_{P3_max}	P3 motor maximum drive torque

3. Modeling

To verify the effectiveness of the energy management strategy, a P1 + P3 plug-in hybrid electric vehicle model was constructed using Cruise (2020) software. The control strategy was implemented in MATLAB/Simulink(R2018b) software for joint simulation validation. The model architecture is illustrated in Figure 5.

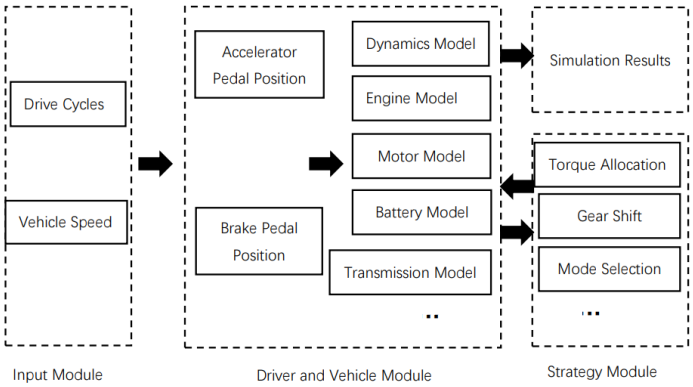

Figure 5. P1 + P3 hybrid powertrain energy management simulation model framework.

3.1. Engine Characteristic Model

Figure 6 illustrates the fuel consumption model of the engine, detailing the fuel consumption of the engine at the corresponding RPM and torque. The data presented were obtained from dynamometer tests.

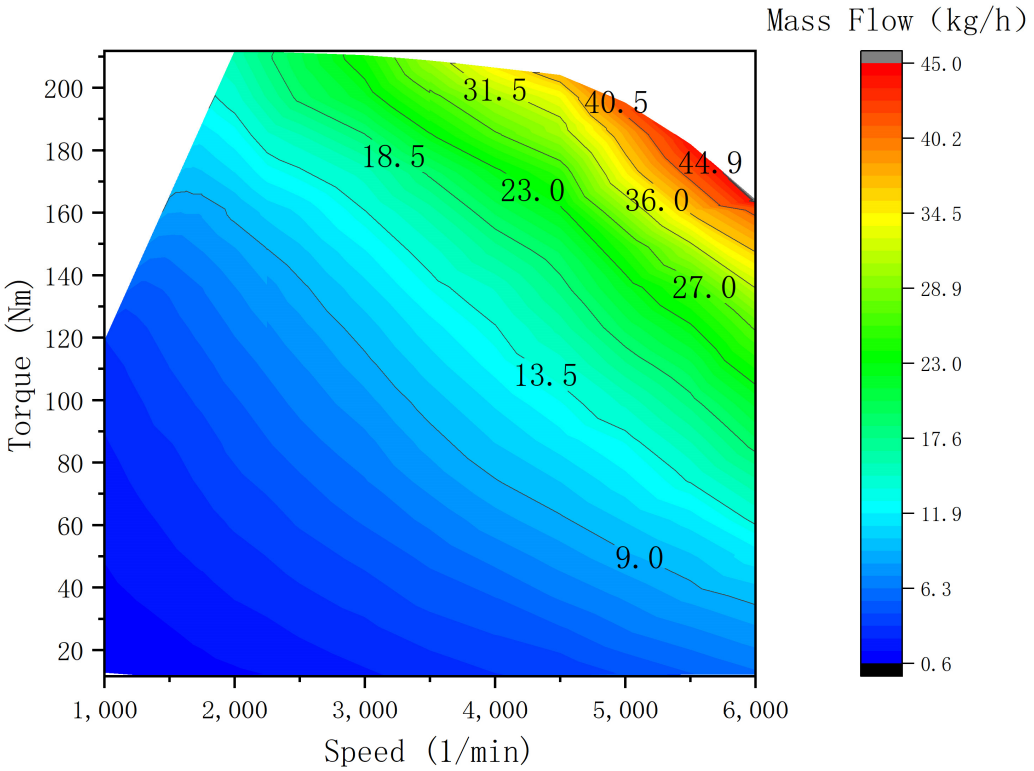

Figure 6. Engine fuel consumption chart.

The methods for calculating fuel consumption rate, engine maximum torque, and fuel consumption for each stage are as follows:

$$b_e = 1000B/P_e \tag{3}$$

$$T_{eng\_max} = f(n_{eng}) \tag{4}$$

$$Q_{eng} = \frac{P_e b_e}{367.1\rho g} \tag{5}$$

In the equations, b_e represents the fuel consumption rate; B represents the hourly fuel consumption; Q_{eng} represents the engine's fuel consumption for each stage; P_e is the engine power; ρ is the density of gasoline; and g represents the acceleration due to gravity.

3.2. Drive Motor Characteristic Model

Similar to the modeling process for the engine, only the external characteristic curves and efficiency of the electric motor are considered [35]. The motor model was established using relevant data obtained from dynamometer tests. Figures 7 and 8 display the external characteristic curves of the P1 and P3 motors.

Figures 9 and 10 illustrate the operational efficiency of the P1 and P3 motors, respectively. The data presented were also obtained from dynamometer tests.

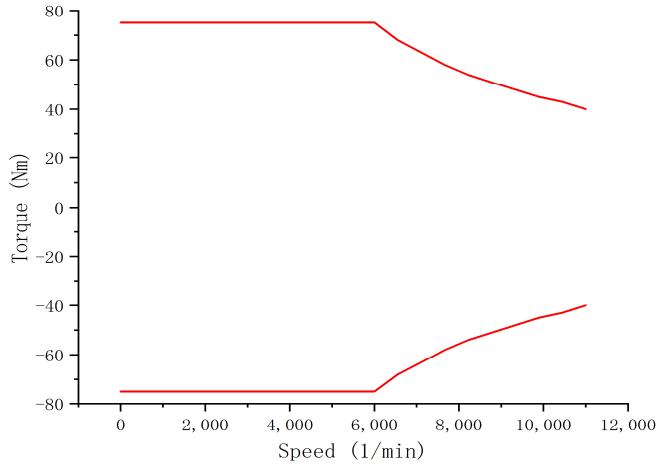

Figure 7. P1 motor external characteristics chart.

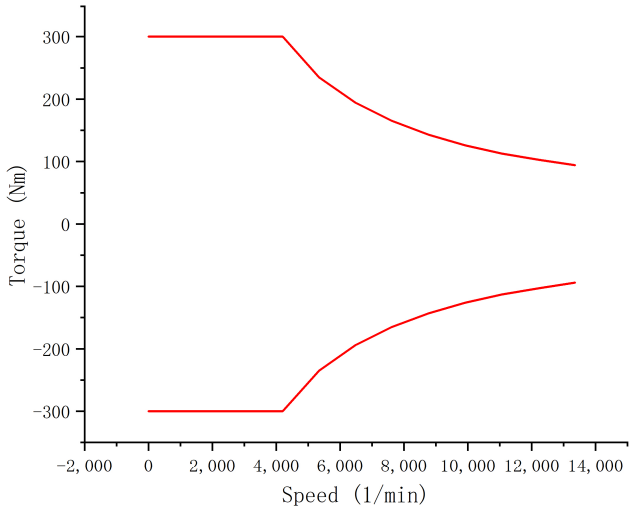

Figure 8. P3 motor external characteristics chart.

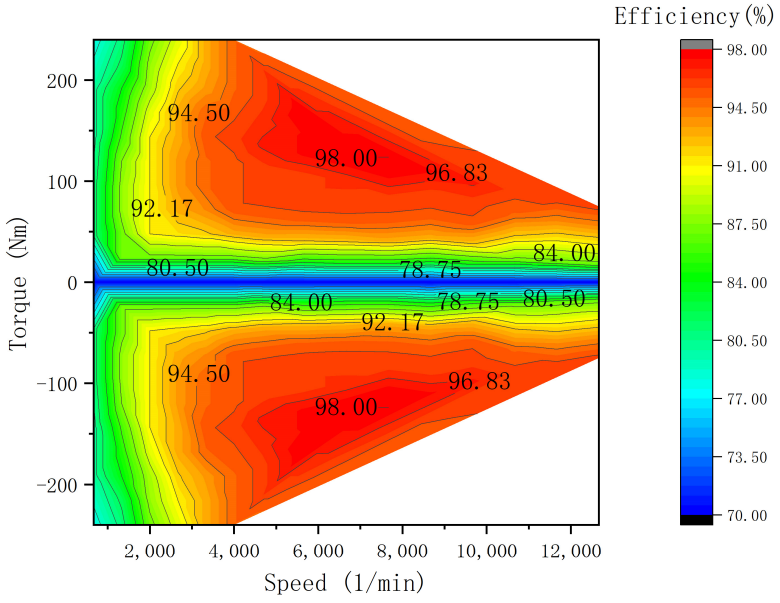

Figure 9. P1 motor efficiency chart.

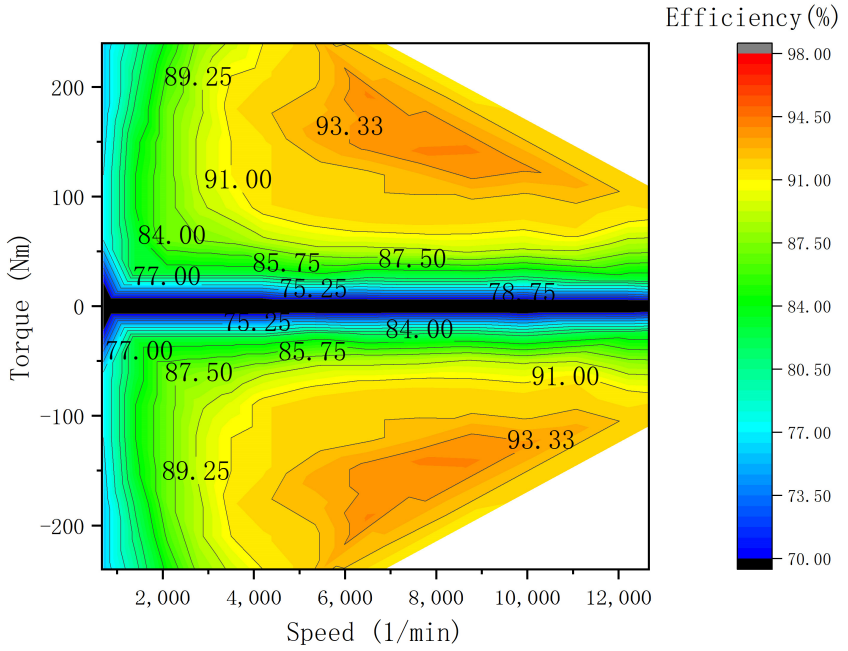

Figure 10. P3 motor efficiency chart.

The formulas for calculating the motor's maximum torque and power are as follows:

$$T_{mot\_max} = f(n_{mot}) \tag{6}$$

$$P_m = \frac{T_{mot} n_{mot}}{9550} \tag{7}$$

Motor power can be expressed as:

$$P_{mot} = \begin{cases} \frac{T_{mot} n_{mot}}{9550} \cdot \eta_{mot}, T_{mot} < 0 \\ \frac{T_{mot} n_{mot}}{9550} \cdot \frac{1}{\eta_{mot}}, T_{mot} \geqslant 0 \end{cases} \tag{8}$$

Motor efficiency is expressed as:

$$\eta_{mot} = f(n_{mot}, T_{mot}) \tag{9}$$

3.3. Power Battery Pack Model

Ignoring the temperature's impact on the power battery, the power battery is simplified into an ideal equivalent circuit model [13]. The equivalent circuit diagram is shown in Figure 11.

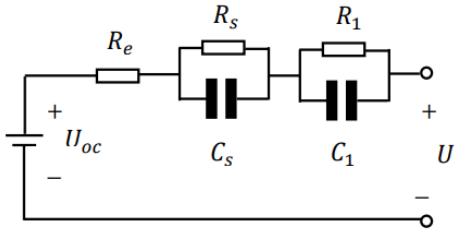

Figure 11. Equivalent circuit diagram of the power battery.

In Figure 11, C_s and C_1 are the polarization capacitors of the battery's polarization internal resistance, representing the hysteresis response of the battery's charge and discharge capacitance [14].

The battery terminal voltage can be calculated using Equation (10):

$$U = U_{oc} - U_s - U_1 - IR_e \tag{10}$$

In the equation, U represents the battery terminal voltage; U_{oc} is the open-circuit voltage of the battery; U_s is the voltage across R_s; U_1 is the voltage across R_1; I represents the battery current; and R_e stands for the internal resistance of the battery.

The formula for the loop current is as follows:

$$I = \frac{U_{oc} - \sqrt{U_{oc}^2 - 4R_{bat}P_{bat}}}{2R_{bat}} \tag{11}$$

In the equation, R_{bat} is the total internal resistance of the battery pack, and P_{bat} is the total power of the battery pack.

When building a power battery model, it should include an SOC calculation module that can reflect the remaining capacity of the battery. The calculation method can utilize the ampere-hour integral method:

$$SOC_t = SOC_0 - \frac{1}{C} \cdot \int_0^t I\, dt \tag{12}$$

In the equation, SOC_0 is the state of charge at the beginning of charging or discharging; SOC_t is the state of charge at time t; and C represents the rated capacity of the battery.

3.4. Vehicle Dynamics Model

In this study, lateral dynamics issues such as turning and lane-changing are excluded. The primary focus is on the vehicle's dynamics and efficiency during straight-line driving. Therefore, wheel rolling resistance, gradient resistance, air resistance, and acceleration resistance are taken into account [15]. The calculation expression for the vehicle dynamics model is as follows:

$$T_F = \frac{r \cdot (mg \cdot sin\theta + mgf \cdot cos\theta + \frac{C_D A v^2}{21.15} + \delta m \cdot du/dt)}{\eta_t} \tag{13}$$

In the equation, m is the total vehicle load; g is the acceleration due to gravity; f is the rolling resistance coefficient; θ is the slope gradient; r is the wheel radius; A is the frontal area; v is the vehicle speed; η_t is the transmission efficiency; and C_D is the drag coefficient.

The Cruise vehicle model is depicted in Figure 12.

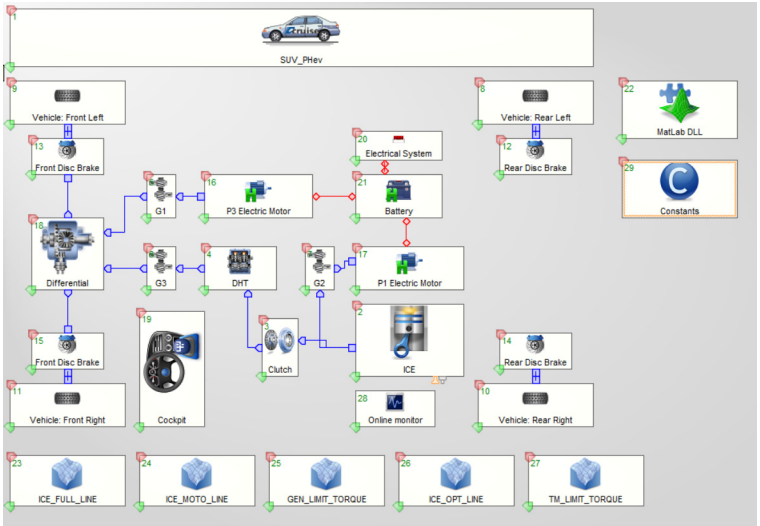

Figure 12. Cruise vehicle model diagram.

The proposed basic parameters of the P1 + P3 structure for the whole vehicle (partial) are shown in Table 5.

Table 5. Partial basic parameters of the research subject.

Project	Parameters	Numerical
Vehicle	Curb weight	2130 kg
	Total mass	2545 kg
	Frontal area	2.26 m^2
	Drag coefficient	0.33
Engine	Engine displacement	1.5 L
	Engine power	105 kW
P1 motor	Peak power	47 kW
	Peak torque	75 Nm
	Maximum RPM	11,000 rpm
P3 motor	Peak power	300 kW
	Peak torque	300 Nm
	Maximum RPM	14,500 rpm
Tires	Rolling radius	287 mm
Transmission	Gear ratio	1:0.75
Power battery	Battery pack capacity	11.52 kWh
	Battery pack rated voltage	320 V

4. Results and Discussion

The simulation was conducted using Cruise and Matlab software for both a conventional gasoline vehicle and P1 + P3 plug-in hybrid electric vehicle.

To more effectively simulate the entire process of PHEV mode switching, three sets of WLTC cycle conditions were combined as the target conditions for simulation. The Worldwide Harmonized Light Vehicles Test Cycle (WLTC) is a globally recognized vehicle test cycle used for measuring fuel consumption, emissions, and the electric range of vehicles. It was developed to provide a more realistic representation of driving conditions compared to the previous test cycle known as the New European Driving Cycle (NEDC). The WLTC consists of a series of driving phases with different average speeds, accelerations, decelerations, and stops. These phases are designed to simulate various driving conditions, including urban, suburban, and extra-urban environments. The cycle aims to reflect real-world driving patterns more accurately, taking into account factors such as traffic congestion, road type, and driving behavior. The initial SOC was set to 0.8, with a maximum SOC limit of 0.8 and a minimum SOC of 0.4.

The vehicle speed tracking performance is shown in Figure 13. It can be observed that the actual vehicle speed trajectory closely follows the WLTC cycle conditions, indicating that the constructed vehicle model and control strategy are correct, and the formulated control strategy exhibits a certain level of stability.

Figure 14: Comparison of engine output torque between conventional vehicle and P1 + P3 dual-motor configuration. The engine output torque of the traditional gasoline vehicle fluctuates significantly with vehicle speed, with a maximum output torque of 240 Nm. In contrast, the engine torque curve of the P1 + P3 dual-motor configuration is more stable. When the vehicle speed is low and the battery is sufficiently charged, the engine remains off, resulting in an output torque of 0. In situations where the battery's state of charge (SOC) is low, and the vehicle enters the range-extender mode, the engine's output torque stabilizes at around 100 Nm. In the high-speed phase where the engine

is the primary power source and maintains SOC stability, the output torque is higher, at approximately 160 Nm.

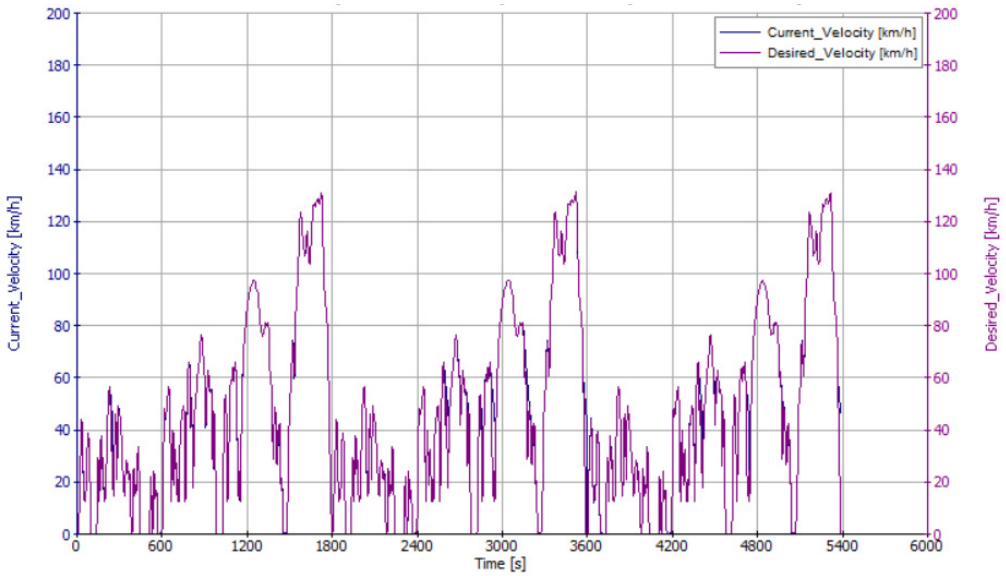

Figure 13. Comparison of actual vehicle speed and target vehicle speed.

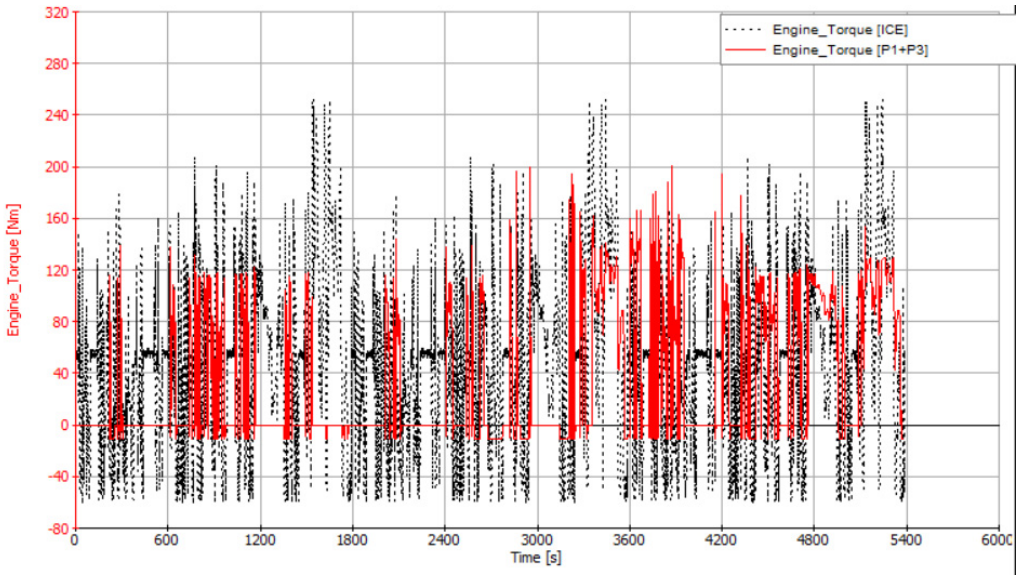

Figure 14. Comparison of engine output torque between conventional vehicle and P1 + P3 du-al-motor configuration.

Figures 15 and 16 illustrate the operating point distribution of the two vehicle models. In the case of the traditional gasoline vehicle, the distribution of engine operating points is relatively scattered, with the majority falling within the low-efficiency range, resulting in poor fuel economy. In contrast, the P1 + P3 dual-motor configuration allows the electric motor to compensate for the engine's output torque when demand is high. Conversely, when torque demand is low, the electric motor functions as a generator, converting a portion of the engine's output torque into electrical energy for recharging the battery. This approach effectively adjusts the engine's operating points, ensuring that it operates more frequently within the high-efficiency range. A clear improvement in engine performance is observed when comparing this configuration to the traditional gasoline vehicle.

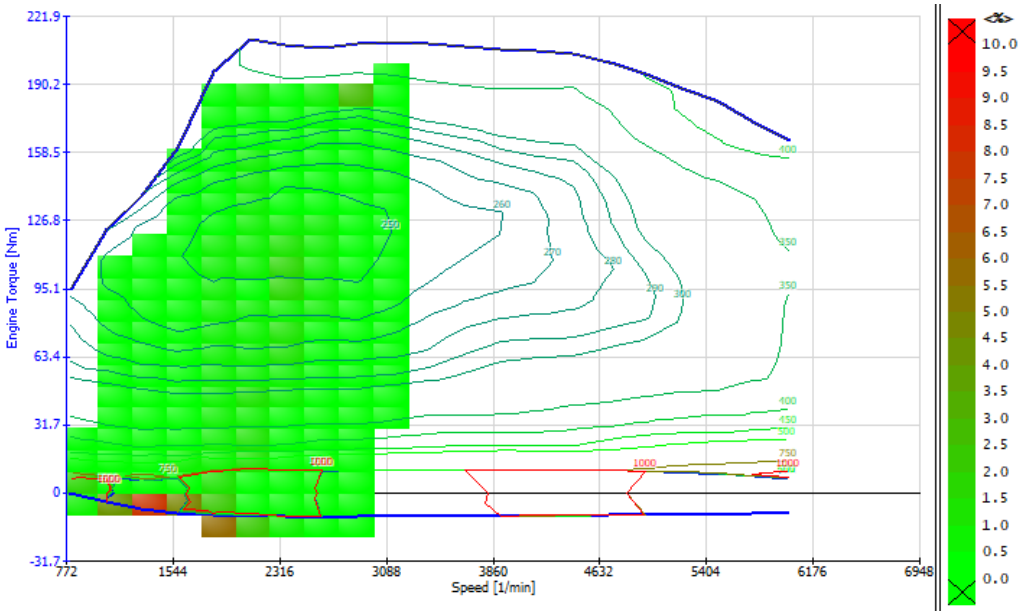

Figure 15. Operating points of the gasoline vehicle engine.

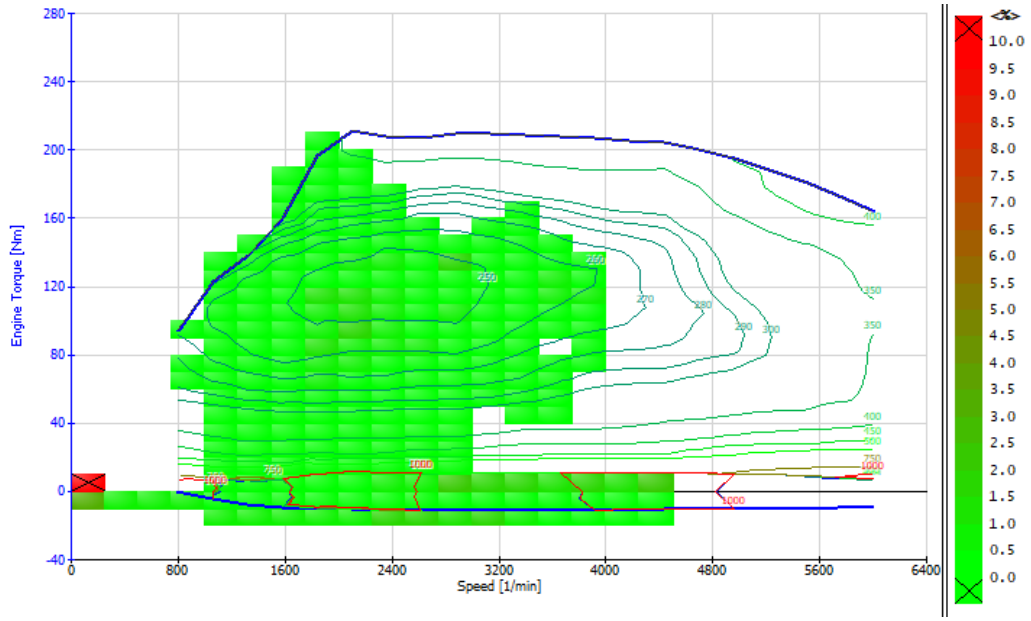

Figure 16. Operating points of the P1 + P3 hybrid powertrain engine.

Figure 17 depicts the speed, torque, and power characteristics of the P1 motor. As shown in the figure, when there is sufficient battery charge during the low-speed stage, the P1 motor remains inactive. When the battery charge is insufficient, the P1 motor operates in conjunction with the engine in a series configuration, entering the range-extending mode to recharge the battery. In the high-speed stage, when the engine's torque output falls short of the vehicle's torque demand, the P1 motor serves as an auxiliary power source, working in parallel with the engine to propel the vehicle. In cases of low battery charge, it enters the power split mode, with the P1 motor and engine working in parallel to recharge the battery.

Figure 18 shows the speed, torque, and power characteristics of the P3 motor. It can be observed that in the mid–low-speed range, the P3 motor serves as the primary power source for the vehicle. During regenerative braking conditions, the P3 motor is engaged in energy recovery, enhancing the fuel economy of the vehicle. The torque variations of different power sources align with the torque distribution rules defined by the control strategy.

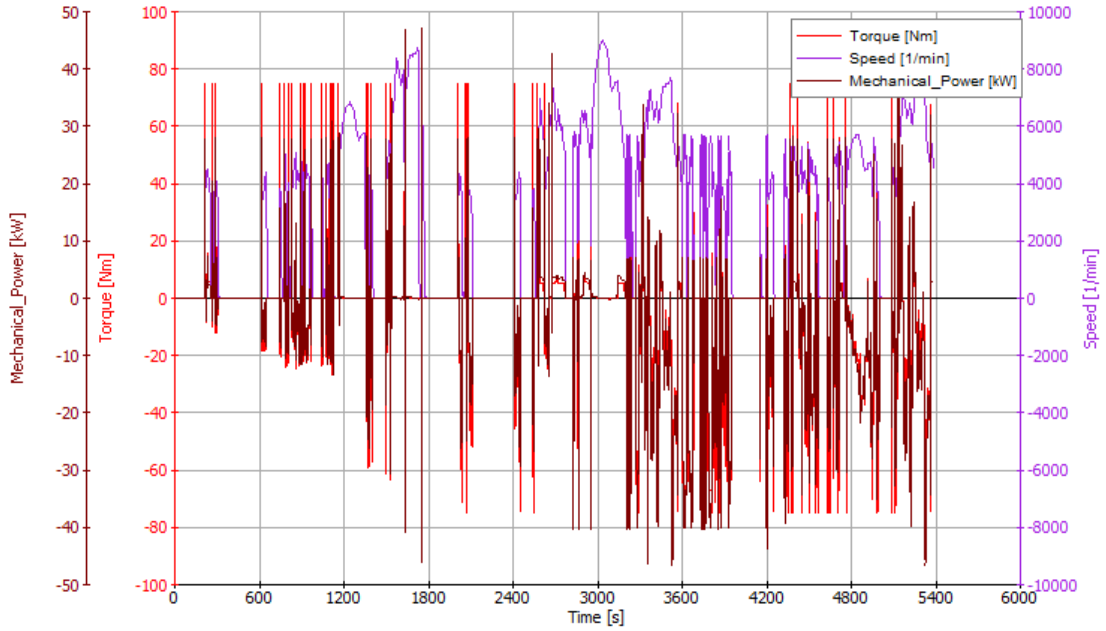

Figure 17. Simulation results of the P1 motor.

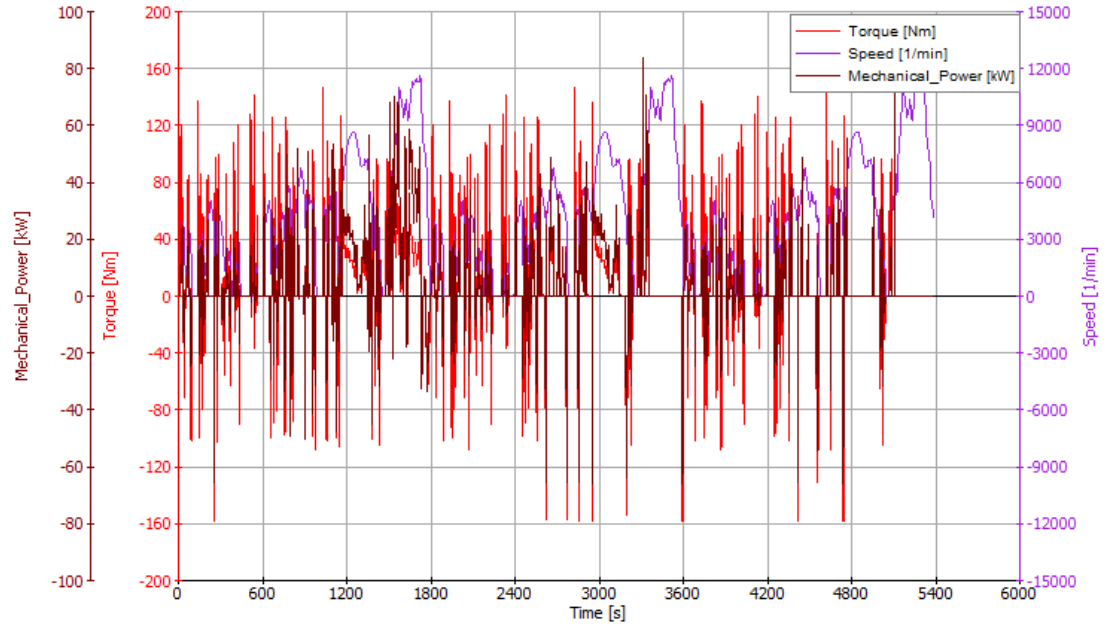

Figure 18. Simulation results for the P3 motor.

Based on the output torque diagrams of the engine and motors, it is evident that the control strategy proposed in this study can reasonably allocate engine and motor torques under various vehicle torque demands, thus meeting the performance requirements in different modes. This indicates that the formulated control strategy is effective and optimized.

Figure 19 shows the variation in the state of charge (SOC) of the power battery. When the battery has a high state of charge, it is prioritized for driving the vehicle, causing the SOC to gradually decrease over time. When the SOC drops to a certain level, the vehicle enters the range-extending mode or the power split mode, with the engine starting to charge the battery. It can be observed that the battery SOC fluctuates between 0.2 and 0.8, and it stabilizes at around 0.4 by the end. This approach significantly reduces battery wear and extends the battery's lifespan.

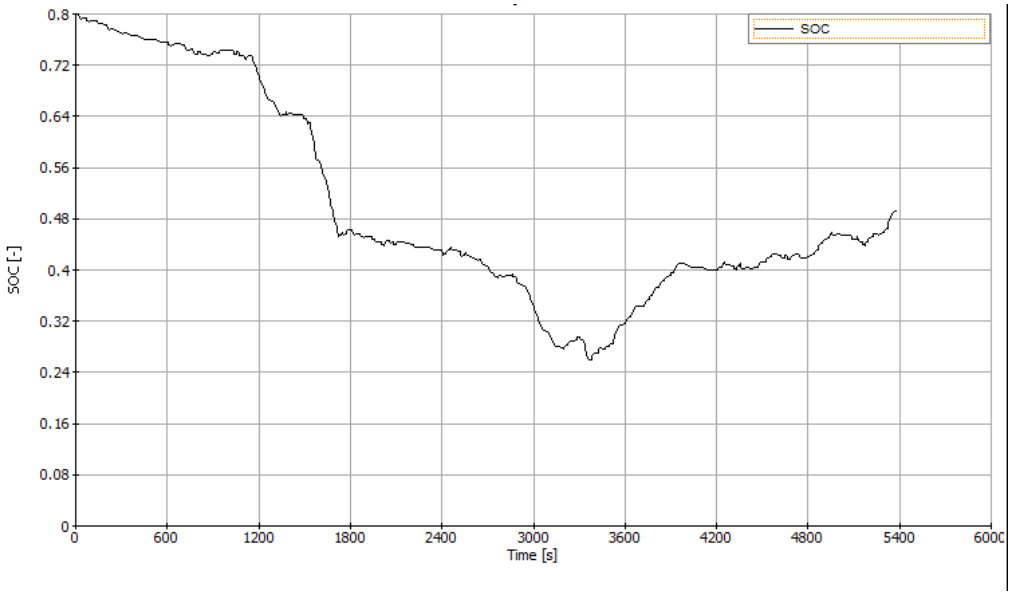

Figure 19. SOC variation curve.

Table 6 presents the final experimental fuel consumption, showcasing a hybrid vehicle utilizing the developed energy management system. The initial state of charge (SOC) stands at 80%, decreasing to 50% by the cycle's end, resulting in a fuel consumption rate of 6.74 L per hundred kilometers. Comparatively, the fuel consumption of a conventional vehicle per hundred kilometers amounts to 10 L. Additionally, Figure 20 provides a more detailed representation of the fuel variations between the two vehicles. It is observed that in the initial phase of hybrid vehicle operation, it primarily relies on the electric motor, resulting in lower and relatively stable fuel consumption. As time progresses, the state of charge (SOC) of the traction battery gradually decreases, and the engine starts to contribute to propulsion and recharge the battery. Consequently, fuel consumption gradually increases, and the rate of fuel consumption significantly accelerates. According to Table 6, the P1 + P3 hybrid configuration (PHEV) demonstrates a 67.4% improvement in fuel efficiency compared to traditional gasoline vehicles, highlighting a substantial enhancement in the vehicle's fuel economy with the introduction of the electric motor.

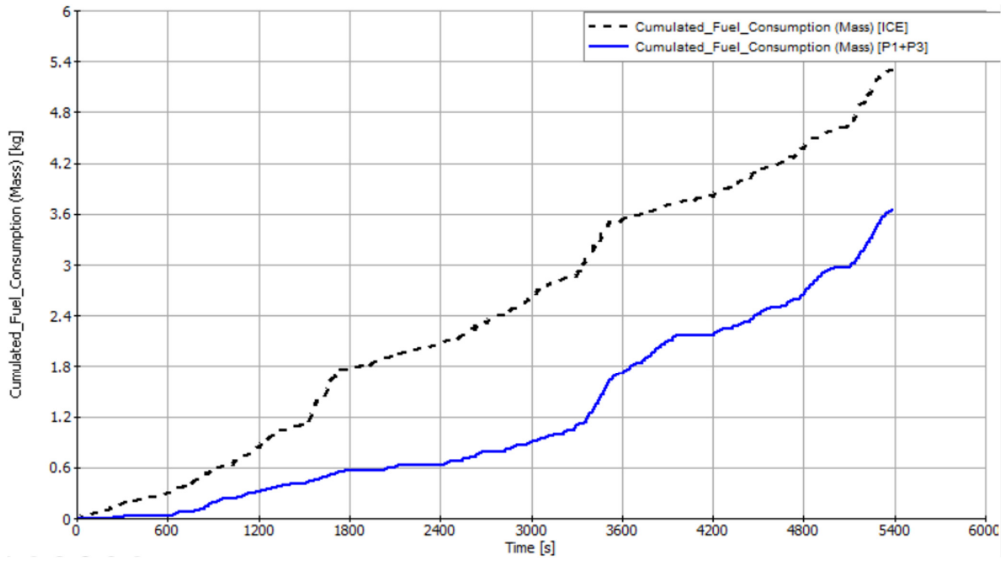

Figure 20. Comparison of fuel consumption.

Table 6. Fuel comparison.

Vehicle Models	Fuel Consumption Per Hundred Kilometers (L)	Fuel Efficiency Gain
Conventional vehicle	10.00	—
P1 + P3 hybrid electric vehicle	6.74	67.4%

5. Conclusions

Taking the P1 + P3 plug-in hybrid electric vehicle (PHEV) configuration as the research subject, a rule-based control strategy was designed on the basis of entire-vehicle modeling. Simulation models of the entire vehicle and control strategy were established using Cruise and MATLAB, and were validated under three combined Worldwide Harmonized Light Vehicles Test Cycle (WLTC) driving cycles. The simulation results included vehicle speed profiles, torque distribution, engine operating points, the current consumption curve, and changes in fuel consumption. The results demonstrated that the developed control strategy effectively coordinated the torque requirements of different driving modes. Compared to conventional gasoline vehicles, the P1 + P3 PHEV configuration showed a significant improvement in fuel economy.

Author Contributions: Conceptualization, B.Z. and P.S.; methodology, B.Z.; software, B.Z.; validation, B.Z.; X.M. and H.L.; formal analysis, Y.Z.; investigation, L.Z.; resources, P.S.; data curation, B.Z.; writing—original draft preparation, B.Z.; writing—review and editing, B.Z. and P.S.; visualization, B.Z.; supervision, P.S.; project administration, P.S.; All authors have read and agreed to the published version of the manuscript.

Funding: This research received no external funding.

Data Availability Statement: The data presented in this study are available on request from the corresponding author. The data are not publicly available due to privacy reasons.

Conflicts of Interest: The authors declare no conflict of interest.

References

1. Chen, L.; Gao, R. Analysis on the Current Status of China's New Energy Vehicle Technology Development. *Transp. Energy Conserv. Environ. Prot.* **2021**, *17*, 14–19.
2. Dižo, J.; Blatnický, M.; Semenov, S.; Mikhailov, E.; Kostrzewski, M.; Droździel, P.; Šťastniak, P. Electric and plug-in hybrid vehicles and their infrastructure in a particular European region. *Transp. Res. Procedia* **2021**, *55*, 629–636. [CrossRef]
3. He, H.; Meng, X. A Review on Energy Management Technology of Hybrid Electric Vehicles. *Trans. Beijing Inst. Technol.* **2022**, *42*, 773–783.
4. Sun, C.; Liu, B.; Sun, F. Review of energy-saving planning and control technology for new energy vehicles. *J. Automot. Saf. Energy* **2021**, *17*, 14–19.
5. Huang, Y.; Surawski, N.C.; Organ, B.; Zhou, J.L.; Tang, O.H.H.; Chan, E.F.C. Fuel consumption and emissions performance under real driving: Comparison between hybrid and conventional vehicles. *Sci. Total Environ.* **2019**, *659*, 275–282. [CrossRef] [PubMed]
6. Tran, D.-D.; Vafaeipour, M.; El Baghdadi, M.; Barrero, R.; Van Mierlo, J.; Hegazy, O. Thorough state-of-the-art analysis of electric and hybrid vehicle powertrains: Topologies and integrated energy management strategies. *Renew. Sustain. Energy Rev.* **2020**, *119*, 109596. [CrossRef]
7. Panday, A.; Bansal, H.O. A review of optimal energy management strategies for hybrid electric vehicle. *Int. J. Veh. Technol.* **2014**, *2014*, 510. [CrossRef]
8. Sabri, M.M.; Danapalasingam, K.; Rahmat, M. A review on hybrid electric vehicles architecture and energy management strategies. *Renew. Sustain. Energy Rev.* **2016**, *53*, 1433–1442. [CrossRef]
9. Shabbir, W. Control Strategies for Series Hybrid Electric Vehicles. Ph.D. Thesis, Imperial College London, London, UK, 2015.
10. Shabbir, W.; Evangelou, S.A. Exclusive operation strategy for the supervisory control of series hybrid electric vehicles. *IEEE Trans. Control. Syst. Technol.* **2016**, *24*, 2190–2198. [CrossRef]
11. Hou, C.; Ouyang, M.; Xu, L.; Wang, H. Approximate Pontryagin's minimum principle applied to the energy management of plug-in hybrid electric vehicles. *Appl. Energy* **2014**, *115*, 174–189. [CrossRef]
12. Liu, T.; Hu, X.; Li, S.E.; Cao, D. Reinforcement learning optimized look-ahead energy management of a parallel hybrid electric vehicle. *IEEE/ASME Trans. Mechatron.* **2017**, *22*, 1497–1507. [CrossRef]

13. Johannesson, L.; Asbogard, M.; Egardt, B. Assessing the potential of predictive control for hybrid vehicle powertrains using stochastic dynamic programming. *IEEE Trans. Intell. Transp. Syst.* **2007**, *8*, 71–83. [CrossRef]
14. Ren, C.; Liu, H. Optimal energy management strategy of plug-in parallel hybrid electric vehicle based on dynamic programming algorithm. *J. Hefei Univ. Technol. (Nat. Sci.)* **2021**, *44*, 1157–1164.
15. Pei, D.; Leamy, M.J. Dynamic programming-informed equivalent cost minimization control strategies for hybrid-electric vehicle. *J. Dyn. Syst. Meas. Control.* **2013**, *135*, 051013. [CrossRef]
16. Zeng, X.; Wang, J. A parallel hybrid electric vehicle energy management strategy using stochastic model predictive control with road grade preview. *IEEE Trans. Control. Syst. Technol.* **2015**, *23*, 2416–2423. [CrossRef]
17. Guercioni, G.R.; Galvagno, E.; Tota, A.; Vigliani, A. Adaptive equivalent consumption minimization strategy with rule-based gear selection for the energy management of hybrid electric vehicles equipped with dual clutch transmission. *IEEE Access* **2020**, *8*, 190017–190038. [CrossRef]
18. Guan, J.C.; Chen, B.C. Adaptive power management strategy based on equivalent fuel consumption minimization strategy for a mild hybrid electric vehicle. In Proceedings of the IEEE Vehicle Power and Propulsion Conference (VPPC), Hanoi, Vietnam, 14–17 October 2019; IEEE: New York, NY, USA, 2019; pp. 1–4.
19. Yu, K.; Yang, H.; Tan, X.; Kawabe, T.; Guo, Y.; Liang, Q.; Fu, Z.; Zheng, Z. Model predictive control for hybrid electric vehicle platooning using slope information. *IEEE Trans. Intell. Transp. Syst.* **2016**, *17*, 1894–1909. [CrossRef]
20. Vidal-Naquet, F.; Zito, G. Adapted optimal energy management strategy for drivability. In *IEEE Vehicle Power and Propulsion Conference*; IEEE: New York, NY, USA, 2012; pp. 358–363.
21. Hannan, M.A.; Azidin, F.A.; Mohamed, A. Multi-sources model and control algorithm of an energy management system for light electric vehicles. *Energy Convers. Manag.* **2012**, *62*, 123–130. [CrossRef]
22. Kim, M.; Jung, D.; Min, K. Hybrid thermostat strategy for enhancing fuel economy of series hybrid intracity bus. *IEEE Trans. Veh. Technol.* **2014**, *63*, 3569–3579. [CrossRef]
23. Panday, A.; Bansal, H.O.; Srinivasan, P. Thermoelectric modeling and online SOC estimation of Li-ion battery for plug-in hybrid electric vehicles. *Model. Simul. Eng.* **2016**, *2016*, 2353521. [CrossRef]
24. Panday, A.; Bansal, H.O. Hybrid electric vehicle performance analysis under various temperature conditions. *Energy Procedia* **2015**, *75*, 1962–1967. [CrossRef]
25. Wang, E.; Ouyang, M.; Zhang, F.; Zhao, C. Performance evaluation and control strategy comparison of supercapacitors for a hybrid electric vehicle. In *Science, Technology and Advanced Application of Supercapacitors*; IntechOpen: London, UK, 2019.
26. Li, Q.; Yang, H.; Han, Y.; Li, M.; Chen, W. A state machine strategy based on droop control for an energy management system of PEMFC-battery-supercapacitor hybrid tramway. *Int. J. Hydrog. Energy* **2016**, *41*, 16148–16159. [CrossRef]
27. Song, K.; Li, F.; Hu, X.; He, L.; Niu, W.; Lu, S.; Zhang, T. Multi-mode energy management strategy for fuel cell electric vehicles based on driving pattern identification using learning vector quantization neural network algorithm. *J. Power Sources* **2018**, *389*, 230–239. [CrossRef]
28. Singh, K.V.; Bansal, H.O.; Singh, D. Feed-forward modeling and real-time implementation of an intelligent fuzzy logic-based energy management strategy in a series–parallel hybrid electric vehicle to improve fuel economy. *Electr. Eng.* **2020**, *102*, 967–987. [CrossRef]
29. Panday, A.; Bansal, H.O. Energy management strategy implementation for hybrid electric vehicles using genetic algorithm tuned Pontryagin's minimum principle controller. *Int. J. Veh. Technol.* **2016**, *2016*, 4234261. [CrossRef]
30. Chen, J.; Xu, C.; Wu, C.; Xu, W. Adaptive fuzzy logic control of fuel-cell-battery hybrid systems for electric vehicles. *IEEE Trans. Ind. Inform.* **2016**, *14*, 292–300. [CrossRef]
31. Singh, K.V.; Bansal, H.O.; Singh, D. Hardware-in-the-loop implementation of ANFIS based adaptive SoC estimation of lithium-ion battery for hybrid vehicle applications. *J. Energy Storage* **2020**, *27*, 101124. [CrossRef]
32. Singh, K.V.; Bansal, H.O.; Singh, D. Development of an adaptive neuro-fuzzy inference system–based equivalent consumption minimisation strategy to improve fuel economy in hybrid electric vehicles. *IET Electr. Syst. Transp.* **2021**, *11*, 171–185. [CrossRef]
33. Hajimiri, M.H.; Salmasi, F.R. A fuzzy energy management strategy for series hybrid electric vehicle with predictive control and durability extension of the battery. In *IEEE Conference on Electric and Hybrid Vehicles*; IEEE: New York, NY, USA, 2006; pp. 1–5.
34. Guo, L. Real-time Optimal Automotive Control for Intelligent Energy Conservation and Road Test. Ph.D. Thesis, Jilin University, Changchun, China, 2019.
35. Wang, B. Research on the Construction of Hybrid Electric Vehicle Driving Condition and the Optimization of Energy Management Strategy. Master's Thesis, Hebei University of Technology, Tianjin, China, 2022.